ACS OMEGA

http://pubs.acs.org/journal/acsodf

Article

Improved Charge Transport across Bovine Serum Albumin–Au Nanoclusters' Hybrid Molecular Junction

Ashwini Nawade,[§] Kumar Babu Busi,[§] Kunchanapalli Ramya, Goutam Kumar Dalapati, Sabyasachi Mukhopadhyay,* and Sabyasachi Chakrabortty*

Cite This: *ACS Omega* 2022, 7, 20906–20913

Read Online

ACCESS | Metrics & More | Article Recommendations | Supporting Information

ABSTRACT: Proteins, a highly complex substance, have been an essential element in living organisms, and various applications are envisioned due to their biocompatible nature. Apart from proteins' biological functions, contemporary research mainly focuses on their evolving potential associated with nanoscale electronics. Here, we report one chemical doping process in model protein molecules (BSA) to modulate their electrical conductivity by incorporating metal (gold) nanoclusters on the surface or within them. The as-synthesized Au NCs incorporated inside the BSA (Au 1 to Au 6) were optically well characterized with UV–vis, time-resolved photoluminescence (TRPL), X-ray photon spectroscopy, and high-resolution transmission electron microscopy techniques. The PL quantum yield for Au 1 is 6.8%, whereas that for Au 6 is 0.03%. In addition, the electrical measurements showed ∼10-fold enhancement of conductivity in Au 6 (8.78×10^{-3} S/cm), where maximum loading of Au NCs was predicted inside the protein matrix. We observed a dynamic behavior in the electrical conduction of such protein-nanocluster films, which could have real-time applications in preparing biocompatible electronic devices.

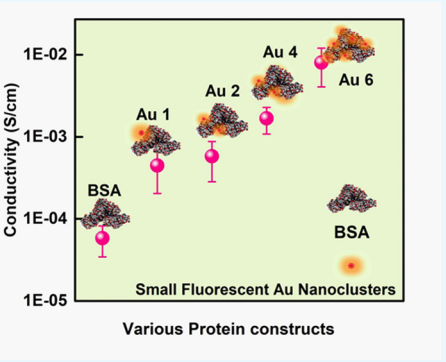

INTRODUCTION

The investigation of newer compounds that showcase semiconductor behaviors in particular organic materials that were once considered insulators has increased tremendously. This rise is due to applications involving specific electronic properties and the persisting desire for miniature and packed electronic devices.[1−4] These materials show some assuring electrical properties as recently improved technology can detect currents/voltage signals at a low operating power.[5] These properties allow the electronic device to be integrated into fabrics, flexible plastic structures, or even miniature bio-devices.[6−9] However, these molecules generally suffer from low long-term stability due to degradation, reactivity with other substances such as water, poor conductivity, and non-biocompatible nature.

Proteins are the most vital life forms that have close relationships with life activities such as nutrition, development, heredity, and metabolism.[9−11] The high specificity of proteins and their biocompatibility make them ideal for various potential applications such as filtering agents, sensors, optical transducers, etc.[9,12,13] Simultaneously, the conduction of ions and electrons over multiple length scales across proteins is significant,[9] and the electron transfer (ET) process of proteins in aqueous solutions and across monolayer configurations on a conducting substrate has been investigated recently.[6,14,15] Multidisciplinary attempts to elucidate the physics and chemistry of charge carriers such as electrons, protons, and ions in the biological charge transfer process have focused primarily on the nano- and microscale electrical or electrochemical transport.[16,17] Different proteins display ET reactions according to their specified function with tunneling over long distances.[10,18] With the success of ET studies across protein monolayers, in the recent past, attempts were made to assimilate proteins into solid-state junctions to understand and compare their electron transfer and electrical conductance properties in both wet electrochemical and solid-state configurations.

The most biologically relevant reactions occur at substrate surfaces and interfaces. These studies could also mimic functional biological components such as enzymes to improve the capacity of the electrocatalytic synthesis used for energy production. It will also help enhance the sensitivity of biomedical sensors, leading to more pharmaceutical applications. In that respect, interfacing biotic and abiotic systems is crucial for developing new bioelectronic technologies. Along with effective transduction of biological signals to electronic circuits, the choice of electronic material is vital as it should be biocompatible and stable under physiological conditions. For this purpose, proteins can be an excellent candidate as they are

Received: March 15, 2022
Accepted: May 25, 2022
Published: June 9, 2022

promising building blocks for most biomaterials and can self-assemble into nanostructures with high tunable electrical properties.[12,17,18] Proteins would demonstrate the convergence of biological materials with synthetic devices by interconverting biological processes and electronic signals.[7,19,20] However, modification/doping of the protein backbone is envisioned to improve their electrical conductivity.[6,10,19,20] In that respect, hybrid nanostructures with nontoxic and noble metal nanoclusters (NCs) would be advantageous.[21−23] They could enhance the charge transport behaviors by reducing influential hopping recombination events.

Herein, we have investigated the charge transport phenomenon of the bovine serum albumin (BSA)−Au NCs hybrid as a model system. BSA, a plasma protein, binds and transports a range of hydrophilic molecules readily adsorbed to surfaces, making it a suitable candidate for custom-built electroactive materials.[24−28] The hybrid Au-nanostructures were synthesized in an aqueous solution using a straightforward bottom-up approach. By varying the precursor concentration, effective loading of Au nanoclusters per BSA molecule was achieved, which significantly influenced their relative photoluminescence (PL) and time-resolved PL properties. Also, the surface compositions of such nanostructures were thoroughly characterized via X-ray photoelectron spectroscopy (XPS). Furthermore, thin films of BSA protein and Au-loaded BSA molecules were subjected to the electrical conductance study to understand how Au NCs alter the electrical conductivity of the protein films, which will make the doped protein viable for future use. We envision developing a protein−metal nanocluster hybrid with a controlled molecular-level doping that can provide new avenues for the rational design of bioelectronic devices with optimized features.

EXPERIMENTAL METHODS

Synthesis of BSA−Au NCs. Aqueous tetrachloroauric (III) acid trihydrate ($HAuCl_4{\cdot}3H_2O$) solution (3 mL, 10 mM) was added to the commercially available BSA solution (3 mL, 40 mg/mL) at the physiological temperature (∼40 °C) under vigorous stirring. The solution was stirred for 5 min, and a pale-yellow color was formed due to the coordination between Au ions and the various functional groups of BSA. Furthermore, NaOH solution (1 M) was added to the reaction mixture to adjust the pH to 12, and the mixture was incubated for 12 h at 40 °C. As a result, the color of the solution turned from pale yellow to deep brown, which confirmed the formation of Au NCs (∼12 h). Next, the as-synthesized BSA−Au NCs were concentrated and washed through a Vivaspin 20 (MWCO30 k) centrifugal concentrator to remove small-molecule impurities. Finally, they were stored at 4 °C before further usage.

Characterization of BSA−Au NCs. Absorption and PL were determined using a TECAN Spark M model microplate reader with a flat-bottom Greiner 96-well plate (200 μL volume) in absorbance and fluorescence intensity scan modes by using a xenon lamp source. Bright-field TEM images were acquired using a JEOL-JEM 2100 high-resolution transmission electron microscope at an accelerating voltage of 200 kV. Five microliters of BSA−Au NC was drop-casted on the holey carbon copper grid and left overnight for water removal. ImageJ software was used for further image analysis. Time-resolved PL measurements were performed using a time-correlated single-photon counting (TCSPC - Horiba Jobin Yvon IBH) spectrometer with a laser diode output at 425 nm as the excitation laser source. The PL decay curves were analyzed using IBH DAS6 software. X-ray photon spectroscopy measurements were done using Al Kα excitation (1486.6 eV) collected in PHI VersaProbe III. The hydrodynamic size measurements were performed in a disposable sizing cuvette, and ζ potential measurements were measured in an electrical double-layered cell using Malvern Zetasizer Nano. The surface composition of the Au NCs labeled with BSA was determined with the X-ray photoelectron spectroscopy technique.

Electrical Characterization of BSA−Au NCs. To measure the electrical conductance across the drop-casted BSA protein film and BSA doped with Au NC films, the Keithley Source Measurement Unit (2636B SYSTEM Source Meter) instrument was utilized, where FTO-coated glass was used as the bottom electrode and eutectic GaIn drops (liquid alloy) were used as the top electrodes (see SI Section S4). The liquid alloy was filled in a microsyringe to ensure a uniform and tiny droplet on the protein film. The volume of the droplet was kept constant in all electrical current−voltage measurements. We estimated the contact area of the EGaIn droplet from the optical images, and the thickness of each film prepared with various protein concentrations was obtained from optical profilometer measurements (see Figure S2 and Table S5). The current−voltage data were acquired for each BSA−Au NC concentration using SMU to calculate the current density−voltage data. To obtain the conductivity of BSA and BSA−Au NC films, MATLAB programming was used for each current density−voltage profile at a low applied bias regime (−0.2 to + 0.2 V). Statistical analysis of variations in conductivity for around 100 junctions of BSA and BSA−Au NC films was carried out with Origin Pro 2016 software.

RESULTS AND DISCUSSION

The globular BSA protein has been studied widely by various researchers for numerous years using varied techniques to illustrate multiple biophysical and biochemical systems. Differential loading of Au NCs on the globular BSA backbone was synthesized by following slight modifications of the literature-reported method. BSA + Au 1 was the lowest loading, and BSA + Au 6 possessed the highest loading of Au NCs[29−31] (*i.e.*, six different loading morphologies). Figure 1a represents the absorbance characteristics of various such BSA−Au hybrid nanostructures, and the absence of surface plasmon resonance absorption demonstrated the possible formation of minor Au NCs (≤2 nm). Additionally, each conjugate retains significant PL properties from Au 1 to Au 6 (see SI Table S1a), as depicted in Figure 1b. However, the PL intensity gets reduced with the relatively higher Au loading on each BSA molecule. Figure 1c represents the digital image of as-synthesized Au NCs without and with ultraviolet light irradiation in the upper and lower panel, respectively, and depicts the PL reduction. From the dynamic light scattering (DLS) data, Table 1 demonstrates an almost similar hydrodynamic size of these samples from BSA + Au 1 to BSA + Au 6. Also, we have carefully excluded the possibility of formation of larger-shaped Au nanoparticles in all of the trials as (a) there was no observable Au surface plasmon peak for large-shaped Au nanoparticles at ∼520 nm; (b) no bigger-sized Au nanoparticles were formed as shown in the DLS data; and (c) all of the samples showed detectable PL behaviors. These observations were in line with previously reported small-sized (∼1.15 to 2.3 nm) Au NCs where various passivating moieties were employed (see SI Table S2). Also, we hypothesized that

https://doi.org/10.1021/acsomega.2c01563
ACS Omega 2022, 7, 20906−20913

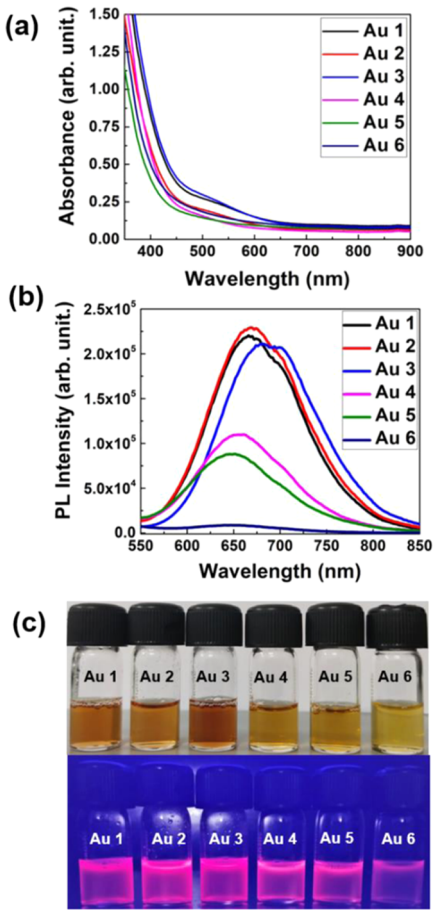

Figure 1. (a, b) Typical absorbance and PL spectra of various Au NCs, where the effective loading of such NCs on each BSA backbone differed. There was no observable plasmonic peak, demonstrating the presence of minor Au NCs in each sample, and subsequent emissions were recorded in the red region. (c) Digital image of those in aqueous solution under room light and UV light (365 nm) in the upper and lower panels.

Table 1. Hydrodynamic Light Scattering Analysis of Those BSA-Conjugated Au NCs (∼10 nm) in which the Existence of a Bigger Size was not Observed[a]

sample name	hydrodynamic size (nm)	ζ potential (mV)
BSA + Au 1	8.878 ± 0.08	−18.76 ± 0.87
BSA + Au 2	8.902 ± 0.68	−22.32 ± 2.29
BSA + Au 3	8.775 ± 2.75	−23.63 ± 0.55
BSA + Au 4	8.284 ± 3.15	−23.76 ± 0.41
BSA + Au 5	7.211 ± 1.31	−22.22 ± 1.70
BSA + Au 6	8.841 ± 0.01	−17.08 ± 1.98

[a]ζ Potential values (∼−20 mV) of those hybrids in an aqueous medium show better colloidal stability.

multiple loading of BSA + Au 6 on each protein molecule might not afford sufficient functional moieties to passivate all of the minor NCs. As a result, a more nonradiative surface trap state may appear, leading to a decrease in PL intensity (Figure 1b). Additionally, their excellent colloidal stability was further confirmed by ζ potential analysis (Table 1), wherein all of the samples exhibited negatively charged species as reported in the literature previously.[32]

To understand the surface composition of the Au NCs labeled with BSA, XPS characterization was carried out. Figure 2a compares the correlated high-resolution Au 4f XPS analysis between Au-BSA hybrids, such as BSA−Au salt mixture, Au 1, Au 4, and Au 6. After deconvolution of those peaks, we confirmed the presence of Au (0) and Au (I) states in our NCs.[29] The topmost plot (Figure 2a) represents physically mixed BSA and Au salt taken as control; the observed binding energy (BE) was almost identical to that of previously reported ones.[33,34] In Au 4f core-level photoemission spectral analysis, surprisingly, we noticed a clear blue shift appearing from Au 1 to Au 6 in the BE values. The peak position/shift change is mainly based on the photoelectron's kinetic energy (KE) change.[35] Au 1 has the higher BE Au $4f_{7/2}$ of ∼83.8 eV in a zero-valent oxidation state due to the decrease in the photoelectron's KE, which maintains the strong bond agreement with neighboring surfactant functional groups. Au 6 possesses a lower BE (∼ 83.3 eV) because of the increased KE of photoelectrons and the weak bonding with surfactant functional groups. The clear blue shift in BE appeared from Au 1 to Au 6 because of the multiple loading of Au NCs in the BSA. The presence of the Au (I) state on the cluster's core surface could be interpreted as an intermediate species. We hypothesized that the tyrosine residues in BSA helped stabilize the NCs inside the reaction solution at a high pH of 12 by partially reducing the Au (I) species to Au (0) valence state during the reduction phase.[36] Interestingly, we noticed the same substantial blue shift in the BE values of the Au (I) (Au $4f_{5/2}$ ∼ 87.4 to 86.9 eV) species due to a steady drop in the reduction from Au 1 to Au 6 owing to the availability of less surfactants again. These observations explained the relative PL intensity behavior from Au 1 to Au 6. Figure 2b determines the full XPS spectrum containing C, N, O, S, and Au peaks at room temperature with a high photon energy ($h\nu$ = 280 eV). We confirmed the existence of the protein by observing the multiple functional groups of C-, N-, and O-related peaks as determined by XPS (see SI Section S3 and Figure S1). Figure 2c describes the improvement in conductivity with the percentage variance in Au (0) and Au (I) oxidation states in different Au-loaded BSA nanostructures. In addition, we observed the highest percentage of Au loading inside the BSA in the Au 6 sample (from overall XPS spectra). Moreover, a higher Au loading possesses more conductivity because of the availability of more hopping sites of metallic Au (0) (∼55%). At a lower Au loading, the conductivity decreases due to the low availability of metallic Au (0) surface area (∼51%).

The high-resolution transmission electron microscopy (HR-TEM) image of BSA + Au 1 in Figure 3a revealed the crystalline nature of the obtained Au NCs within or on the surfaces of the BSA molecules. The characteristic lattice spacing between two Au crystal planes is 0.24 nm, confirming the formation of Au's (111) plane. Also, the average size of the clusters was calculated to be 1.84 ± 0.15 nm (∼25 number of counts). The BSA + Au 6 samples were dropcasted for HRTEM measurements to better understand their size. However, they imposed more difficulties in identifying the background BSA protein and separated the minor Au NCs. Figure 3b represents the temperature-dependent PL spectra of the Au 1 sample, where a decrease in PL intensity was observed as the temperature increased. As we know, a suitable environment would impart better colloidal stability. We believed that raising the temperature might open many nonradiative relaxation trap states, which results in PL quenching. This phenomenon was further substantiated through a time-resolved PL lifetime study (see SI Figure S3).

https://doi.org/10.1021/acsomega.2c01563
ACS Omega 2022, 7, 20906−20913

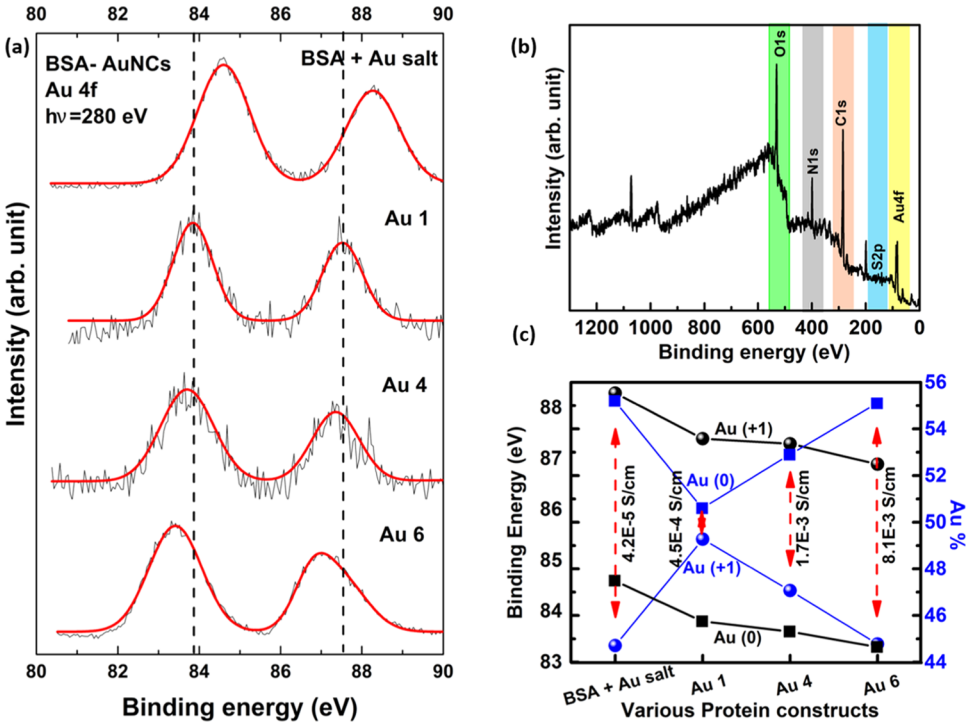

Figure 2. XPS analysis of BSA−Au NCs. (a) Au 4f core-level photoemission profiles of Au NCs passivated in protein at room temperature with $h\nu$ = 280 eV photon energy. Three different concentrations of Au NCs were used for binding energy studies, ranging from BSA + Au 1 to BSA + Au 6, and BSA + Au salt was used as for the control surface analysis. High-resolution XPS revealed the existence of Au $4f_{7/2}$ and Au $4f_{5/2}$ binding energies attributed to Au (0) zero-valent and Au (+1) monovalent oxidation states. (b) Representative BSA−Au NCs' XPS full survey spectrum, where the BSA + Au 1 sample was taken for analysis. (c) The improvement of conductivity was investigated by determining the percentages of Au (0) and Au (+1) in various protein constructions and measuring their binding energies. The square-shaped and spherical points denote the characteristics of Au (0) and Au (1), respectively. Also, the blue and black colors represent the percentage of Au loading and binding energy, respectively.

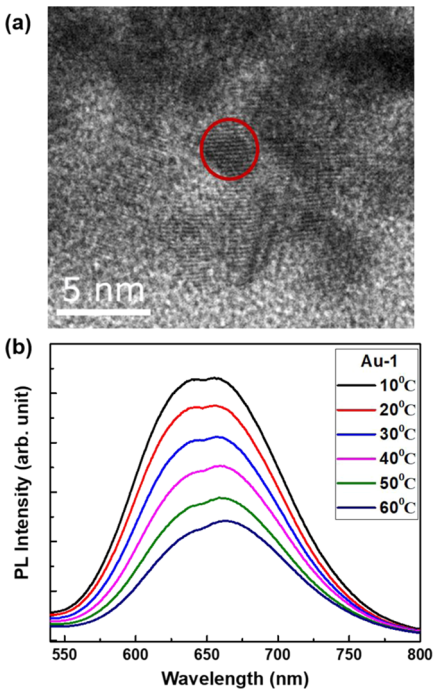

Figure 3. (a) A typical HR-TEM image of BSA−Au NCs showing the crystalline nature of NCs, where the lattice spacing of the Au (111) plane (0.24 nm) was evident. (b) Temperature-dependent PL spectrum of a representative Au 1 sample, where the PL intensity decreased with increasing temperature.

Furthermore, in the temperature range between 10 and 60 °C, the presence of appreciable fluorescence proved that the small Au NCs were not coalescent with each other, which might have a significant impact on their use in the charge transport phenomenon across protein thin films at elevated temperature. Also, we believe that at ∼60 °C, BSA may be denatured but did not affect the fluorescent properties of any of our synthesized NCs (See SI Figure S4).

The most crucial factor for using any material in bioelectronics would be its long-term stability. We have performed the PL stability test of as-synthesized BSA−Au hybrid nanostructures with 15-month-old samples. As depicted in Figure 4a, no decrease in fluorescent intensity was observed, ascertaining our synthesis protocol's robustness and subsequent stability. Time-resolved PL (TRPL) measurement was performed to determine the origin of the PL observed. As shown in Figure 4b, systematic shortening of the lifetime is observed when the effective Au loading is increased in each BSA backbone. The decay profiles of four representative samples, *i.e.*, Au 1, Au 2, Au 4, and Au 6, were presented according to the overall trends seen in their relative PL intensity.

We observed a triple lifetime decay curve for each sample, which is comparable with the literature (see Table S1b).[37] A significant decrease in phosphorescence or longer PL lifetimes in Au 6 compared to Au 1, *i.e.*, from 1×10^{-6} to 9.45×10^{-10} s were recorded. This might be attributed to the fact that more nonradiative pathways may open due to the poor surface passivation of Au NCs in Au 6. Over a few decades, experimental and theoretical studies of electron transport

https://doi.org/10.1021/acsomega.2c01563
ACS Omega 2022, 7, 20906−20913

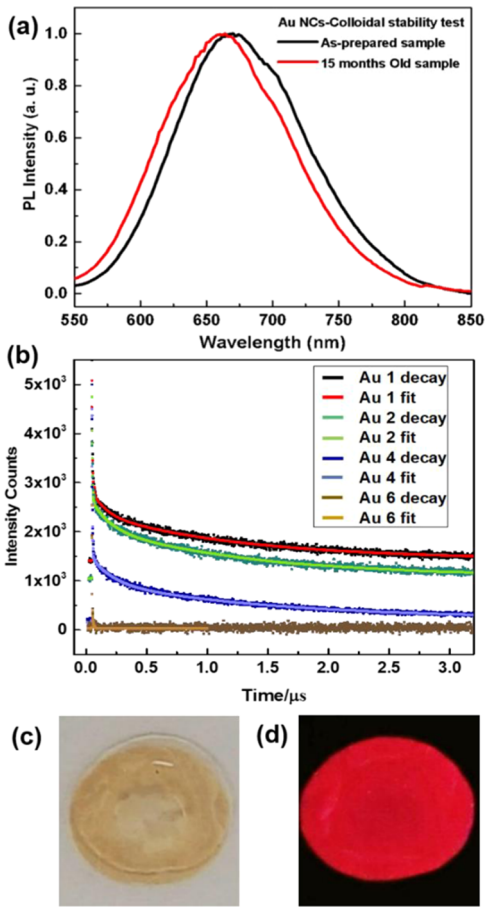

Figure 4. (a) Stability test for the as-synthesized Au 1 sample stored in water; even after 15 months, the PL intensity was not reduced. (b) Time-resolved PL lifetime decay patterns of four different BSA−Au hybrids, namely Au 1, Au 2, Au 4, and Au 6. Au NCs with increased Au loading showed a progressive reduction of the radiative lifetime. Representative digital image of BSA−Au NCs (40 mg/mL) on glass substrate—(c) in room light and (d) in UV light (365 nm) irradiation (only for visual illustration).

have concluded that energy-activated hopping is the most dominant electron transport process across nearly insulating biofilms. So, the electrical conductance across virtually insulating protein films can be further improved by incorporating more hopping rates inside the solid-state protein films. In analogy with conducting polymer films, hopping rates are governed mainly by the distance between successive hopping sites (traps) and the carrier lifetime at each hopping site. The reduction of PL lifetime when we populated the BSA molecules with more Au NCs in the ultrafast lifetime PL decay measurements (see Table 1 and SI Section S7) depicts that Au NCs attached to the BSA backbone function as electron trap centers. Following our observation of the reduction of PL lifetime with increased effective Au NCs in each BSA molecule, we postulated that small Au clusters attached to the BSA backbone could emulate hopping sites for electrical conductions.

The electrical characteristics of BSA protein and BSA−Au hybrid nanostructure films were investigated to explore the effect of self-assembled conjugated Au NCs across the BSA films. The electrical transport characteristics in terms of the normalized current density (current per unit contact area, Figure S2) were measured as a function of the applied voltage ($J-V$, see SI Section S8) across the thin films prepared from solutions of BSA and BSA−Au NC hybrid (Au 1 to Au 6) material, containing varied concentrations of BSA (*i.e.*, 12.5, 6.25, and 2.5 mg/mL). We have carefully eliminated the statistical variations of the measured current densities, which could originate from variations of junction area, film thicknesses, and impurities at the junction interface, by collecting more than hundreds of data sets for each BSA concentration. These $J-V$ data were analyzed using MATLAB programming to obtain the electrical conductivity

$$\left(G \times L/A_{\text{measured}}\ \text{in}\frac{\text{S}}{\text{cm}};\ G - \text{conductance},\ L - \text{film thickness},\ A_{\text{measured}} - \text{contact area}\right)$$

of BSA and BSA−Au hybrid (Au 1−Au 6) material thin films. Since the maximum occurrence of electrical conductivity was not symmetrical, we have performed logarithmic distribution to obtain the statistical means of ∼100 junctions (see SI Sections S8 and S9).

As seen in Figure 5a, the effective increase of Au NCs in a BSA molecule positively impacts the electrical conductivity by

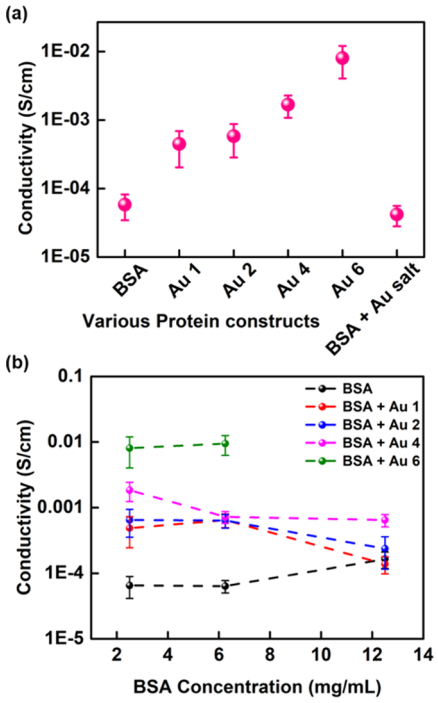

Figure 5. (a) Comparison analysis of the conductivity of various BSA−Au NCs. The protein concentration was fixed in each case at 2.5 mg/mL. (b) Variation of BSA−Au film conductivity with different concentrations, where the error bar represents variation over ∼100 junctions.

around 100 times higher than the control samples (BSA or BSA without Au NCs). We have carefully excluded the use of *large plasmonic Au nanoparticles* in this case as they would act as metallic behavior and recombination centers, and the original contribution from the BSA protein would be suppressed. The most occurring electrical conductivity (*i.e.*, over ∼100 measurements) for films prepared with 2.5 mg/mL BSA protein (by diluting with 50 mg/mL BSA) was recorded as 6.55×10^{-5} S/cm, whereas the same concentration of BSA

https://doi.org/10.1021/acsomega.2c01563
ACS Omega 2022, 7, 20906−20913

protein with self-assembled Au 1 depicted 4.87×10^{-4} S/cm, which is enhanced by orders of magnitude (Figure 5a). Furthermore, the electrical conductivities for BSA−Au 2, Au 4, and Au 6 nanocluster hybrid films were 6.44×10^{-4}, 1.84×10^{-3}, and 8.78×10^{-3} S/cm, respectively, which are comparable with the intrinsic silicon conductivity.[38] Films made of the BSA−Au 6 sample exhibit the highest electrical conductivity and have a higher effective number of Au NCs self-assembled on the surface or beneath each BSA molecule. The enhancement in electrical conductivity originates from the efficient flow of electrons through the BSA protein backbone and the attached Au cluster that act as hopping sites. To support our hypothesis, the control experiments were carried out, where we introduced gold salt/ions without the reducing agent so that no initiation of NC formation occurred. In the absence of the Au nanocluster's assembly, the electrical conductivity of films prepared with the BSA−Au salt (*marked as Control in* Figure 5a) resembles the electrical conductivity of typical BSA films (*marked as BSA*). The XPS data (Figure 2c) supports the claim as the Au (0) and Au (I) percentages are almost the same for the BSA + Au salt and BSA + Au 6. Still, there is a significant enhancement in the conductivity, which is attributed to the incorporation of Au NCs inside the protein matrix.

In analogy with conducting polymer films, a material's universal nature, i.e., electrical conductivity, depends on the carrier hopping rates, primarily governed by the distance between successive hopping sites (traps) and the carrier lifetime at each hopping site. The measured PL decay lifetimes starting with BSA−Au 1 to BSA−Au 6 depict the reduction in the distance between suggestive Au NCs (considering distance-dependent energy transfer processes within the Au NCs), which further manifested as higher hopping rates across the films. To confirm the universality of the electrical conduction mechanism across BSA−Au nanocluster films, we have prepared films of controlled thicknesses by varying the protein concentrations to explore the electrical properties of these films. Figure 5b represents the variation of electrical conductivity across BSA−Au NC films, where we varied the protein concentrations with a constant doping level of Au NCs to individual BSA molecules. BSA and BSA−Au 6 films depict a uniform electrical conductivity across the various thicknesses of the films, whereas we observed a variation in conductivity for other Au doping levels. The electrical conductivity reduces with protein concentrations for BSA−Au 1 to BSA−Au 4. The reduction in electrical conductance could originate from the nonuniform doping across the films, which needs further investigation. A detailed characterization of the carrier transport mechanism through the BSA protein films with and without Au NC would require combining spectroscopic techniques and an analysis of the temperature and humidity dependence of the electrical conductivity.

However, our overall results demonstrate the emergence of an electronic charge transport across protein films when Au nanoclusters were self-assembled on the surface or within the protein molecules. Therefore, an enhanced conductance of protein films is required in high-end applications, such as adhesives to the immune-responsive tissues.[1,11,39] Our obtained electrical conductivity of protein films is significant in characterizing many biochemical reactions and determining the usability of biomolecules in sensors and nanoelectronics circuitry.

CONCLUSIONS

In conclusion, we have successfully synthesized atomically precise bright fluorescent BSA−Au hybrid nanostructures. The effective loading of small Au NCs on each BSA was varied, and the outcome of their optical-electrical properties was thoroughly investigated. Protein-Au hybrid nanostructures provided good passivation for better colloidal stability of the hybrid, and they were stable in an aqueous solution for about 15 months. The low PL intensity trend from BSA + Au 1 to BSA + Au 6 was further substantiated through their time-resolved PL decay lifetimes. Gold nanostructures (BSA + Au 1 to BSA + Au 6) have considerably enhanced electrical conductance compared to bare BSA protein in thin-film devices. The electrical conductance showed a linear increase when a lower protein concentration was taken into consideration in the case of the BSA−Au hybrid nanostructured thin films. We envision that the molecular-level understanding of the charge transport behavior of such a protein−metal nanocluster hybrid will provide new avenues for the rational design of bioelectronic devices with optimized features. The BSA−Au cluster has been a promising model for bioelectronic functionalities. With an increase in their current carrying capacity, they can be used for many more applications, especially as the interface between the tissue and organ in biocompatible devices.

ASSOCIATED CONTENT

Supporting Information

The Supporting Information is available free of charge at https://pubs.acs.org/doi/10.1021/acsomega.2c01563.

Synthesized Au NCs in BSA protein using various dopant concentrations, XPS characterization conducted for elemental composition, UV−visible absorbance and PL characteristics of control samples followed by temperature-dependent PL measurements performed for stability studies, average current density−voltage plots for different BSA−Au NCs hybrids, electrical conductivity bar graphs for data analysis of BSA−Au NCs thin films (PDF)

AUTHOR INFORMATION

Corresponding Authors

Sabyasachi Mukhopadhyay − *Department of Physics, SRM University, AP - Andhra Pradesh, Guntur, Andhra Pradesh 522240, India;* orcid.org/0000-0002-6290-6380; Email: sabyasachi.m@srmap.edu.in

Sabyasachi Chakrabortty − *Department of Chemistry, SRM University, AP - Andhra Pradesh, Guntur, Andhra Pradesh 522240, India;* orcid.org/0000-0002-2759-2208; Email: sabyasachi.c@srmap.edu.in

Authors

Ashwini Nawade − *Department of Physics, SRM University, AP - Andhra Pradesh, Guntur, Andhra Pradesh 522240, India*

Kumar Babu Busi − *Department of Chemistry, SRM University, AP - Andhra Pradesh, Guntur, Andhra Pradesh 522240, India*

Kunchanapalli Ramya − *Department of Physics, SRM University, AP - Andhra Pradesh, Guntur, Andhra Pradesh 522240, India*

https://doi.org/10.1021/acsomega.2c01563
ACS Omega 2022, 7, 20906−20913

Goutam Kumar Dalapati − *Department of Physics, SRM University, AP - Andhra Pradesh, Guntur, Andhra Pradesh 522240, India*

Complete contact information is available at: https://pubs.acs.org/10.1021/acsomega.2c01563

Author Contributions

§A.N. and K.B.B. contributed equally to this work. S.C. and S.M. conceived the idea. A.N. and K.B.B. performed the experiments and analyzed the obtained data. K.R. and G.K.D. were involved in analyzing the data. Finally, S.C. and S.M. wrote the manuscript along with A.N. and K.B.B.

Notes

The authors declare no competing financial interest.

■ ACKNOWLEDGMENTS

This work is supported by SRM University Startup Research funding and SERB-DST, Govt. of India, under Early Career Research Award Grants (ECR/2017/001937). The authors acknowledge the support from MNRE (Project No. 31/03/2014-15/PVSE-R&D) for the development of the HR-TEM facility at SRMIST.

■ REFERENCES

(1) Davis, J. J.; Morgan, D. A.; Wrathmell, C. L.; Axford, D. N.; Zhao, J.; Wang, N. Molecular Bioelectronics. *J. Mater. Chem.* **2005**, *15*, 2160.

(2) Carroll, R. L.; Gorman, C. B. The Genesis of Molecular Electronics. *Angew. Chem., Int. Ed.* **2002**, 23.

(3) Ratner, M. A. Introducing Molecular Electronics. *Mater. Today* **2002**, *5*, 20−27.

(4) Nichols, R. J.; Haiss, W.; Higgins, S. J.; Leary, E.; Martin, S.; Bethell, D. The Experimental Determination of the Conductance of Single Molecules. *Phys. Chem. Chem. Phys.* **2010**, *12*, 2801.

(5) Bostick, C. D.; Mukhopadhyay, S.; Pecht, I.; Sheves, M.; Cahen, D.; Lederman, D. Protein Bioelectronics: A Review of What We Do and Do Not Know. *Rep. Prog. Phys.* **2018**, *81*, No. 026601.

(6) Waleed Shinwari, M.; Jamal Deen, M.; Starikov, E. B.; Cuniberti, G. Electrical Conductance in Biological Molecules. *Adv. Funct. Mater.* **2010**, *20*, 1865−1883.

(7) Aviram, A.; Ratner, M. A. Molecular Rectifiers. *Chem. Phys. Lett.* **1974**, *29*, 277−283.

(8) Mentovich, E.; Belgorodsky, B.; Gozin, M.; Richter, S.; Cohen, H. Doped Biomolecules in Miniaturized Electric Junctions. *J. Am. Chem. Soc.* **2012**, *134*, 8468−8473.

(9) Ron, I.; Pecht, I.; Sheves, M.; Cahen, D. Proteins as Solid-State Electronic Conductors. *Acc. Chem. Res.* **2010**, *43*, 945−953.

(10) Ron, I.; Sepunaru, L.; Itzhakov, S.; Belenkova, T.; Friedman, N.; Pecht, I.; Sheves, M.; Cahen, D. Proteins as Electronic Materials: Electron Transport through Solid-State Protein Monolayer Junctions. *J. Am. Chem. Soc.* **2010**, *132*, 4131−4140.

(11) Zhang, B.; Song, W.; Pang, P.; Lai, H.; Chen, Q.; Zhang, P.; Lindsay, S. Role of Contacts in Long-Range Protein Conductance. *Proc. Natl. Acad. Sci. U.S.A.* **2019**, *116*, 5886−5891.

(12) de la Rica, R.; Matsui, H. Applications of Peptide and Protein-Based Materials in Bionanotechnology. *Chem. Soc. Rev.* **2010**, *39*, 3499.

(13) Zhang, D.; Liu, Q. Biosensors and Bioelectronics on Smartphone for Portable Biochemical Detection. *Biosens. Bioelectron.* **2016**, *75*, 273−284.

(14) Rosenberg, B. Electrical Conductivity of Proteins. II. Semiconduction in Crystalline Bovine Hemoglobin. *J. Chem. Phys.* **1962**, *36*, 816−823.

(15) Mukhopadhyay, S.; Karuppannan, S. K.; Guo, C.; Fereiro, J. A.; Bergren, A.; Mukundan, V.; Qiu, X.; Castañeda Ocampo, O. E.; Chen, X.; Chiechi, R. C.; McCreery, R.; Pecht, I.; Sheves, M.; Pasula, R. R.; Lim, S.; Nijhuis, C. A.; Vilan, A.; Cahen, D. Solid-State Protein Junctions: Cross-Laboratory Study Shows Preservation of Mechanism at Varying Electronic Coupling. *iScience* **2020**, *23*, No. 101099.

(16) Nishinaka, T.; Takano, A.; Doi, Y.; Hashimoto, M.; Nakamura, A.; Matsushita, Y.; Kumaki, J.; Yashima, E. Conductive Metal Nanowires Templated by the Nucleoprotein Filaments, Complex of DNA and RecA Protein. *J. Am. Chem. Soc.* **2005**, *127*, 8120−8125.

(17) Altamura, L.; Horvath, C.; Rengaraj, S.; Rongier, A.; Elouarzaki, K.; Gondran, C.; Maçon, A. L. B.; Vendrely, C.; Bouchiat, V.; Fontecave, M.; Mariolle, D.; Rannou, P.; Le Goff, A.; Duraffourg, N.; Holzinger, M.; Forge, V. A Synthetic Redox Biofilm Made from Metalloprotein−Prion Domain Chimera Nanowires. *Nat. Chem.* **2017**, *9*, 157−163.

(18) Mukhopadhyay, S.; Gärtner, W.; Cahen, D.; et al. Electron Transport via a Soluble Photochromic Photoreceptor. *Phys. Chem. Chem. Phys.* **2016**, *18*, 25671−25675.

(19) Lebedev, N.; Griva, I.; Blom, A.; Tender, L. M. Effect of Iron Doping on Protein Molecular Conductance. *Phys. Chem. Chem. Phys.* **2018**, *20*, 14072−14081.

(20) Yu, J.; Chen, Y.; Xiong, L.; Zhang, X.; Zheng, Y. Conductance Changes in Bovine Serum Albumin Caused by Drug-Binding Triggered Structural Transitions. *Materials* **2019**, *12*, 1022.

(21) Shang, L.; Brandholt, S.; Stockmar, F.; Trouillet, V.; Bruns, M.; Nienhaus, G. U. Effect of Protein Adsorption on the Fluorescence of Ultrasmall Gold Nanoclusters. *Small* **2012**, *8*, 661−665.

(22) Banerjee, C.; Kuchlyan, J.; Banik, D.; Kundu, N.; Roy, A.; Ghosh, S.; Sarkar, N. Interaction of Gold Nanoclusters with IR Light Emitting Cyanine Dyes: A Systematic Fluorescence Quenching Study. *Phys. Chem. Chem. Phys.* **2014**, *16*, 17272.

(23) Waszkielewicz, M.; Olesiak-Banska, J.; Comby-Zerbino, C.; Bertorelle, F.; Dagany, X.; Bansal, A. K.; Sajjad, M. T.; Samuel, I. D. W.; Sanader, Z.; Rozycka, M.; Wojtas, M.; Matczyszyn, K.; Bonacic-Koutecky, V.; Antoine, R.; Ozyhar, A.; Samoc, M. PH-Induced Transformation of Ligated Au_{25} to Brighter Au_{23} Nanoclusters. *Nanoscale* **2018**, *10*, 11335−11341.

(24) Amdursky, N.; Pecht, I.; Sheves, M.; Cahen, D. Doping Human Serum Albumin with Retinoate Markedly Enhances Electron Transport across the Protein. *J. Am. Chem. Soc.* **2012**, *134*, 18221−18224.

(25) Amdursky, N.; Ferber, D.; Pecht, I.; Sheves, M.; Cahen, D. Redox Activity Distinguishes Solid-State Electron Transport from Solution-Based Electron Transfer in a Natural and Artificial Protein: Cytochrome C and Hemin-Doped Human Serum Albumin. *Phys. Chem. Chem. Phys.* **2013**, *15*, 17142.

(26) Amdursky, N.; Wang, X.; Meredith, P.; Riley, D. J.; Payne, D. J.; Bradley, D. D. C.; Stevens, M. M. Electron Hopping Across Hemin-Doped Serum Albumin Mats on Centimeter-Length Scales. *Adv. Mater.* **2017**, *29*, No. 1700810.

(27) Agam, Y.; Nandi, R.; Kaushansky, A.; Peskin, U.; Amdursky, N. The Porphyrin Ring Rather than the Metal Ion Dictates Long-Range Electron Transport across Proteins Suggesting Coherence-Assisted Mechanism. *Proc. Natl. Acad. Sci. U.S.A.* **2020**, *117*, 32260−32266.

(28) Mejias, S. H.; López-Martínez, E.; Fernandez, M.; Couleaud, P.; Martin-Lasanta, A.; Romera, D.; Sanchez-Iglesias, A.; Casado, S.; Osorio, M. R.; Abad, J. M.; González, M. T.; Cortajarena, A. L. Engineering Conductive Protein Films through Nanoscale Self-Assembly and Gold Nanoparticles Doping. *Nanoscale* **2021**, *13*, 6772−6779.

(29) Xie, J.; Zheng, Y.; Ying, J. Y. Protein-Directed Synthesis of Highly Fluorescent Gold Nanoclusters. *J. Am. Chem. Soc.* **2009**, *131*, 888−889.

(30) Chakrabortty, S.; Sison, M.; Wu, Y.; Ladenburger, A.; Pramanik, G.; Biskupek, J.; Extermann, J.; Kaiser, U.; Lasser, T.; Weil, T. NIR-Emitting and Photo-Thermal Active Nanogold as Mitochondria-Specific Probes. *Biomater. Sci.* **2017**, *5*, 966−971.

(31) Sison, M.; Chakrabortty, S.; Extermann, J.; Nahas, A.; James Marchand, P.; Lopez, A.; Weil, T.; Lasser, T. 3D Time-Lapse Imaging and Quantification of Mitochondrial Dynamics. *Sci. Rep.* **2017**, *7*, No. 43275.

(32) Han, L.; Xia, J.-M.; Hai, X.; Shu, Y.; Chen, X.-W.; Wang, J.-H. Protein-Stabilized Gadolinium Oxide-Gold Nanoclusters Hybrid for Multimodal Imaging and Drug Delivery. *ACS Appl. Mater. Interfaces* **2017**, *9*, 6941−6949.
(33) Tanaka, A.; Takeda, Y.; Nagasawa, T.; Takahashi, K. Chemical States of Dodecanethiolate-Passivated Au Nanoparticles: Synchrotron-Radiation Photoelectron Spectroscopy. *Solid State Commun.* **2003**, *126*, 191−196.
(34) Casaletto, M. P.; Longo, A.; Martorana, A.; Prestianni, A.; Venezia, A. M. XPS Study of Supported Gold Catalysts: The Role of Au0 and Au+δ Species as Active Sites. *Surf. Interface Anal.* **2006**, *38*, 215−218.
(35) X-ray Photoelectron Spectroscopy (XPS) Reference Pages: An Overview of X-ray Photoelectron Spectroscopy. http://www.xpsfitting.com/2012/08/an-overview-of-x-ray-photoelectron.html (accessed Feb 13, 2022).
(36) Le Guével, X.; Hötzer, B.; Jung, G.; Hollemeyer, K.; Trouillet, V.; Schneider, M. Formation of Fluorescent Metal (Au, Ag) Nanoclusters Capped in Bovine Serum Albumin Followed by Fluorescence and Spectroscopy. *J. Phys. Chem. C* **2011**, *115*, 10955−10963.
(37) Xu, Y.; Sherwood, J.; Qin, Y.; Crowley, D.; Bonizzoni, M.; Bao, Y. The Role of Protein Characteristics in the Formation and Fluorescence of Au Nanoclusters. *Nanoscale* **2014**, *6*, 1515−1524.
(38) Pauleau, Y.; Barna, P. B. *Protective Coatings and Thin Films: Synthesis, Characterization, and Applications*, 1st ed.; Nato Science Partnership Subseries; Springer, 1997.
(39) Choi, J.-W.; Oh, B.-K.; Kim, Y. J.; Min, J. Protein-Based Biomemory Device Consisting of the Cysteine-Modified Azurin. *Appl. Phys. Lett.* **2007**, *91*, No. 263902.

https://doi.org/10.1021/acsomega.2c01563
ACS Omega 2022, 7, 20906−20913